

Intrinsic emergence of Majorana modes in Luttinger $j = \frac{3}{2}$ systems

Julian Benedikt Mayer, Miguel A. Sierra , and Ewelina M. Hankiewicz*

*Institute for Theoretical Physics and Astrophysics and Würzburg-Dresden Cluster of Excellence ct.qmat,
University of Würzburg, Am Hubland, 97074 Würzburg, Germany*



(Received 30 March 2022; accepted 10 June 2022; published 23 June 2022)

We analyze theoretically two different setups for s -wave superconductivity proximitized $j = \frac{3}{2}$ particles in Luttinger materials that are able to host Majorana bound states (MBSs). First, we consider a one-dimensional superconductor (SC) wire with intrinsic bulk inversion asymmetry (BIA). In contrast to wires, modeled by a quadratic dispersion with Rashba spin-orbit coupling, there are two topological phase transitions in our systems at finite magnetic fields. Second, we analyze a two-dimensional Josephson junction on the Luttinger model finding a topological region even in the absence of BIA and Rashba spin-orbit couplings. This originates from the hybridization of the light and heavy hole bands of the $j = \frac{3}{2}$ states in combination with the SC pairing. As a consequence, both systems can be driven into a topological phase hosting MBSs. Hence, we predict that MBSs form in any SC proximitized Josephson junction on two-dimensional Luttinger materials by the application of magnetic field alone. This opens an avenue for the search of topological SC.

DOI: [10.1103/PhysRevB.105.224513](https://doi.org/10.1103/PhysRevB.105.224513)

I. INTRODUCTION

Remarkable interest in Majorana bound states (MBSs) has arisen in recent decades [1–5]. In condensed-matter systems, they manifest as zero-energy modes appearing at the boundaries of a topological superconductor (SC) [6,7]. Since they come in pairs to form a fermionic state, they acquire nonlocal properties which topologically protect them from decoherence [4–9]. For this reason, MBSs are ideal candidates for topological quantum computation. Consequently, several experiments attempt to detect signatures of MBSs [3,10–13].

It has been predicted that a semiconducting nanowire with s -wave proximitized superconductivity and spin-orbit coupling (SOC) can host MBSs at its boundaries [5,14–18]. These appear in a topological phase after a Zeeman field, perpendicular to the SOC field, inverts the SC gap. Similarly, a two-dimensional Josephson junction with perpendicular Zeeman and SOC fields is also able to host MBSs at the boundary between the normal region and the vacuum [12,13,19–21]. These MBSs appear, if the double degenerate Andreev bound states (ABSs) split at finite Zeeman fields, giving rise to a topological regime between two crossings. The topological gap in the ABS spectrum protects the MBSs against perturbations.

In this paper, we analyze these setups for the $j = \frac{3}{2}$ states of bulk materials such as HgTe, α -Sn, or half-Heusler compounds, which exhibit a quadratic band touching at the Γ point around the Fermi energy. These so-called quadratic nodal semimetals can be described within the four-band Luttinger model (LM) [22,23]. Luttinger materials display a rich variety of topological phases induced by perturbations, i.e., in the presence of strain they are three-dimensional topological

insulators [24–26] or topological semimetals [22,27–30], with local attractive electron-electron interaction they transform into superconducting phase [31,32], and they can show higher spin SC pairings [33–39]. Our models are appealing for two reasons: on the one hand, they give a more realistic description of materials. On the other hand, the LM can be derived from the $\mathbf{k} \cdot \mathbf{p}$ model in which spin-orbit interactions, especially bulk inversion asymmetry (BIA) terms, are already taken into account [40]. Hence, MBSs could emerge intrinsically with no extra implementations of spin-orbit interactions in the setup.

Specifically, we show that in a one-dimensional (1D) LM wire, MBSs emerge from the interplay between intrinsic BIA and the Zeeman field. Further, in contrast to the semiconducting Rashba nanowires, the topological phase in our systems is limited to a finite Zeeman field range. Moreover, we predict that for two-dimensional (2D) Josephson junctions on Luttinger materials, MBSs still appear due to the intrinsic SOC originating from the mixing between light hole (LH) and heavy hole (HH) bands. Therefore, in Josephson junctions on 2D materials described by $j = \frac{3}{2}$ particles no extra SOC is necessary to generate MBSs.

II. THEORETICAL MODELS

We use the two-dimensional four-band LM [41] to describe the $j = \frac{3}{2}$ states of our systems:

$$\hat{H}_L(\mathbf{k}) = \alpha_0 k^2 \hat{1}_4 + \alpha_z \hat{M}_z(\mathbf{k}) + \alpha_{\square} \hat{M}_{\square}(\mathbf{k}) - \mu \hat{1}_4, \quad (1)$$

with $\hat{M}_z(\mathbf{k}) = \frac{5}{2} k^2 \hat{1}_4 - 2(\mathbf{k} \cdot \hat{\mathbf{J}})^2$ and $\hat{M}_{\square}(\mathbf{k}) = k_x^2 \hat{J}_x^2 + k_y^2 \hat{J}_y^2 - \frac{2}{5}(\mathbf{k} \cdot \hat{\mathbf{J}})^2 - \frac{1}{5} k^2 \hat{\mathbf{J}}^2$. Here, $\mathbf{k} = (k_x, k_y, 0)$ is the momentum; $\hat{\mathbf{J}} = (\hat{J}_x, \hat{J}_y, \hat{J}_z)$ are the $j = \frac{3}{2}$ spin matrices; and α_0 , α_z , and α_{\square} are material-specific parameters related to the effective masses of the bands while μ is the chemical potential. We emphasize

*hankiewicz@physik.uni-wuerzburg.de

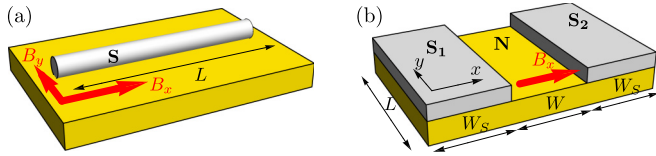


FIG. 1. Sketch of the setups: (a) A one-dimensional Luttinger wire of length L in contact with an s -wave superconductor and in the presence of a Zeeman field B_x or B_y . (b) A two-dimensional Josephson junction of length L with a Zeeman field applied in a normal region of width W . Two s -wave superconductors of width W_S and phases $\phi_{S_1} = -\phi/2$ and $\phi_{S_2} = \phi/2$, respectively, separated by a normal regime N on top of the Luttinger material.

that the α_z and α_{\square} terms involve an intrinsic symmetric SOC in the system for at least two dimensions [33].

Using the Nambu basis $(c_{3/2}, c_{1/2}, c_{-1/2}, c_{-3/2}, -c_{-3/2}^\dagger, c_{-1/2}^\dagger, c_{1/2}^\dagger, c_{3/2}^\dagger)$, where $c_{j_z}^\dagger$ (c_{j_z}) are the creation (annihilation) operators of particles with z components of total angular momentum j_z , we get the Bogoliubov–de Gennes (BdG) Hamiltonian describing a 1D SC wire [Fig. 1(a)]

$$\hat{H}_W(k_x) = \hat{\tau}_z \hat{H}_L(k_x)|_{k_y=0} + \hat{\tau}_z \hat{H}_{\text{BIA}}(k_x) + \Delta \hat{\tau}_x \hat{1}_4 + B_y \hat{\tau}_0 \hat{J}_y, \quad (2)$$

where $\hat{\tau} = (\hat{\tau}_x, \hat{\tau}_y, \hat{\tau}_z)$ are the Pauli matrices in Nambu space. The second term corresponds to the BIA $\hat{H}_{\text{BIA}}(k_x) = \beta k_x \{\hat{J}_x, \hat{J}_y^2 - \hat{J}_z^2\}$, where β is the BIA strength and $\{\dots\}$ is the anticommutator. We identify \hat{H}_{BIA} as an intrinsic source of SOC interactions in any semimetal of the \mathbf{T}_d tetrahedral symmetry group. The proximitized SC is represented by the induced s -wave pairing potential Δ . In addition, a Zeeman term B_y is applied perpendicularly to the BIA field.

For the 2D Josephson junction [Fig. 1(b)], we consider the Hamiltonian

$$\hat{H}_{JJ}(\mathbf{k}) = \hat{\tau}_z \hat{H}_L(\mathbf{k}) + \hat{H}_\Delta^{JJ} + \hat{\tau}_0 \hat{H}_Z^{JJ}. \quad (3)$$

In this setup, two SCs (S_1 and S_2) are separated by a non-SC (N) region of width W . Therefore, the SC coupling takes the form $\hat{H}_\Delta = \Delta \Theta(|x| - W/2) [e^{i\phi(x)} \hat{\tau}_+ + e^{-i\phi(x)} \hat{\tau}_-] \hat{1}_4$ where $\Theta(x)$ is the Heaviside function, $\phi(x) = (\phi/2) \text{sgn}(x)$ is the SC phase, and $\hat{\tau}_\pm = (\hat{\tau}_x \pm i\hat{\tau}_y)/2$. Additionally, the Zeeman field is only applied in the normal region such that $\hat{H}_Z^{JJ} = \Theta(W/2 - |x|) B_x \hat{J}_x$.

In the presence of a Zeeman field, our systems have broken time-reversal symmetry and conserved particle-hole symmetry. Therefore, they are in the symmetry class D [42,43] which is categorized by the topological invariant $\mathcal{Q} = \det(r)$ in 1D, where r is the reflection matrix [44,45]. We notice that, even though the Josephson junction is a 2D system, the normal region in which the MBSs appear can be considered as a quasi-1D wire since the MBSs are localized along the y direction only. Therefore, we obtain the topological invariant of both setups by employing the method for one dimension explained in Ref. [45].

The solutions to the scattering problem and BdG equation were calculated numerically using the KWANT package [46].

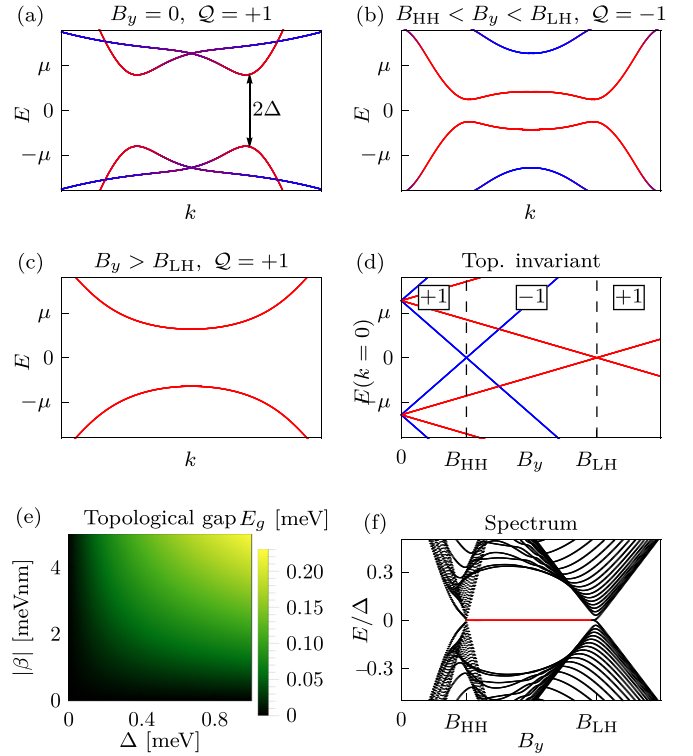


FIG. 2. (a)–(d) Bulk band-structure calculations of an infinite wire with proximitized superconductivity and Zeeman field B_y [see Fig. 1(a)], using the parameters of HgTe $(\alpha_0, \alpha_z, \alpha_{\square}) = (16.58, 9.36, -1.6) \frac{\hbar^2}{2m}$ and $\beta = -4.31$ meV nm [47,48]. We set the chemical potential at $\mu = 0.25$ meV and $\Delta = 0.2$ meV. The color code indicates the character of the bands being light-hole (red) or heavy-hole (blue) like. The insets in (d) specify the topological invariant \mathcal{Q} . The critical magnetic fields B_{HH} and B_{LH} are given in Eq. (4). (e) Size of the minimum gap for all momenta as a function of the superconducting gap Δ and the strength of the bulk inversion asymmetry β in the topological phase at $B_y = (B_{\text{HH}} + B_{\text{LH}})/2$. (f) Band structure of a wire with finite length L as a function of B_y with a system size much larger than the localization length of the MBS ($L \gg \lambda$). States localized at the boundaries of the wire are indicated in red, showing the Majorana bound states in the topologically nontrivial region.

III. SUPERCONDUCTING WIRE

In comparison with the two-band Rashba model, the four-band LM considers double degenerate LH and HH states. We show that the interplay of these two types of states in the LM gives rise to intriguing physics. The LM can describe both semimetal ($|\alpha_0| < |2\alpha_z - 3/5\alpha_{\square}|$) and metal ($|\alpha_0| > |2\alpha_z - 3/5\alpha_{\square}|$) regimes, where the LH and HH states have either opposite or the same curvature.

For the sake of simplicity, we study the band structure of the SC wire focusing on semimetals ($|\alpha_0| < |2\alpha_z - 3/5\alpha_{\square}|$) and $\mu > 0$, where the Fermi energy only lies in the LH band [Fig. 2(a)]. In the absence of a Zeeman field, the SC coupling Δ opens a gap in all states around the Fermi energy and we are in a trivial phase with $\mathcal{Q} = +1$. Applying a Zeeman field B_y breaks the time-reversal symmetry of the system. Consequently, the bands will split into positive and negative energies depending on their spin degeneracy. One can find a

critical Zeeman field for each band where a topological phase transition occurs. This is caused by a band crossing at zero momentum. Such critical fields are given by

$$B_{\text{HH}} = \frac{2}{3}\sqrt{\Delta^2 + \mu^2}, \quad B_{\text{LH}} = 2\sqrt{\Delta^2 + \mu^2}. \quad (4)$$

For $k = 0$, the critical Zeeman field $B_y = B_{\text{HH}}$ corresponds to a crossing between the quasielectron and quasihole states in the BdG Hamiltonian for the $j_z = -3/2$ bands. This crossing yields a topological transition to a nontrivial phase characterized by a topological invariant $\mathcal{Q} = -1$ [Fig. 2(b)]. The second critical field $B_y = B_{\text{LH}}$ denotes a band crossing between the quasielectron and quasihole states for the $j_z = -1/2$ bands. In this regime, the system undergoes a second topological transition and returns to a trivial phase $\mathcal{Q} = +1$ [Fig. 2(c)]. The existence of two topological transitions can be used as an additional knob to identify MBSs in experiments such as in Ref. [51]. This last feature cannot be observed in two-band wires with Rashba or Dresselhaus SOC [14,15] since more than one topological transition can only occur in systems with more than two bands.

We note that in the absence of BIA, the system is gapless [see Fig. 2(e)]. In one dimension, the α_z and α_{\square} terms do not act as SOC and only give a difference in the effective masses of the $|j_z| = \frac{1}{2}$ and $|j_z| = \frac{3}{2}$ states (see the Supplemental Material [52]). This is due to a simple fact that squared components of total angular and spin momenta give a constant. Therefore, the gap cannot be opened with only the application of Zeeman fields and BIA has to be included as a source of SOC to find topological features in the system. High BIA strengths will enhance the topological gap. Hence, we expect the formation of MBSs in a wide range of materials from the T_d symmetry class.

Due to the bulk-boundary correspondence [53], the nontrivial topological invariant implies that we have a MBS localized at the edges of the wire. Using tight-binding calculations, we show in Fig. 2(f), that such zero-energy states indeed appear in the nontrivial region for $L \gg \lambda$, where λ is the localization length of the MBS [5]. As expected, the MBS at each end of a shorter wire hybridizes and yields Majorana oscillations around zero energy.

Similar results can be also obtained by considering Rashba SOC instead of BIA. However, we focus here on BIA since it is an intrinsic property of the material, while Rashba SOC has to be generated by an applied electric field or asymmetric quantum well structure. We note that if Rashba SOC is considered in the 1D wire along the x axis [Fig. 1(a)], one requires a different direction of the Zeeman field (B_x) [14,15].

IV. TWO-DIMENSIONAL JOSEPHSON JUNCTION

In 2D Josephson junctions, the propagating particles in the N region experience multiple Andreev reflections at the NS interfaces giving rise to ABSs that are confined to the N region [$|x| \leq W/2$; see Fig. 1(b)] [20,21]. We first focus on the $k_y = 0$ case of an infinite L system, making the junction effectively 1D. In the absence of a Zeeman field, those ABSs are degenerate. An in-plane Zeeman field applied to the N region breaks the time-reversal symmetry and lifts the degeneracy of the ABS [Fig. 3(b)]. This leads to two zero-energy

crossings at critical phase differences, indicating an effective inversion of the gap and a change in the topology. Therefore, the energy gap as a function of Zeeman field and phase difference [see Fig. 3(c)] gives a topological phase diagram which can be alternatively obtained by calculating the topological invariant \mathcal{Q} . In a perfect system, without normal reflection at the NS interface, the topological region is centered around the Thouless energy ($E_T = \frac{\pi}{2} \frac{\hbar v_F}{W} = 2.2$ meV). Since the SC regions in our system have a finite length much larger than the coherence length [54], we find a small contribution of normal reflection, which affects the topological phase diagram. It was shown [23] that any semi-infinite 2D Luttinger semimetal with a single edge and without cubic anisotropy ($\alpha_{\square} = 0$) hosts either one (for $1 \leq |\alpha_0|/|\alpha_z| < 2$) or two (for $|\alpha_0|/|\alpha_z| < 1$) edge states, originating from the quadratic node in the bulk band structure. Metallic Luttinger materials ($|\alpha_0|/|\alpha_z| > 2$) do not host edge states. In this work, we focus on semimetals with one edge state at positive energies, using the material-specific parameters of α -Sn ($\alpha_0/\alpha_z = 1.57$) shown in Fig. 3(a). For such materials, the sign of μ is important and can be used to tune the system into different topological phases. In the subgap energy range ($|E| < |\Delta|$), the transmission in the N region is only given by the $j_z = \pm 3/2$ states for $\mu < 0$ and determined by a combination of $j_z = \pm 1/2$ and edge states for $\mu > 0$. From now on, we focus on the $\mu < 0$ phase, without edge states.

Having a topological phase, which can host Majorana bound states, demands additionally a finite gap at all transverse momenta k_y . Interestingly, we find such gaps at all points in the topological region of Fig. 3(d) away from $\phi = 0$, even without additional inversion symmetry breaking by BIA or Rashba terms. Previously, 2D Josephson junctions built from semiconductors were modeled by a two-dimensional electron gas, where an additional inversion symmetry breaking Rashba or Dresselhaus term was needed to open a topological gap [12,20,21,55]. In the Luttinger semimetal, the intrinsic SOC of the α_z and α_{\square} terms is $k_x k_y \{J_x, J_y\}$ [52]. This term in combination with a finite phase difference between the SCs opens a topological gap with a nontrivial topological invariant under magnetic field.

Considering a system that is confined in y direction with a finite length L allows us to study the wave functions of the states in real space. We show the density of the lowest-energy wave functions in the different regions of the topological phase diagram in Figs. 3(e)–3(h) at $\phi = 1.2\pi$. In the trivial region for small magnetic fields, we find ABSs which are bound to the normal conducting region at $|x| \leq W/2$ [Fig. 3(e)] in the induced SC gap. For magnetic fields in the topological region with $\mathcal{Q} = -1$, we find a single zero-energy state which is additionally localized in y direction giving rise to a MBS [Fig. 3(f)]. The localization length of the MBS is proportional to the inverse of the topological gap [$E_g^{\text{top}}(\phi, B_x) = \min_{k_y} E_g(\phi, B_x, k_y)$]. For increasing magnetic fields, the gap of the ABS closes again at $k_y = 0$ and provides a second band inversion with the transition to trivial SC ($\mathcal{Q} = +1$). Here, we find two zero-energy states which are localized in y direction [Figs. 3(g) and 3(h)] combining to a trivial conventional fermion.

Figures 3(i) and 3(j) show calculations for the conductance of the system around the edge of the N region. Here,

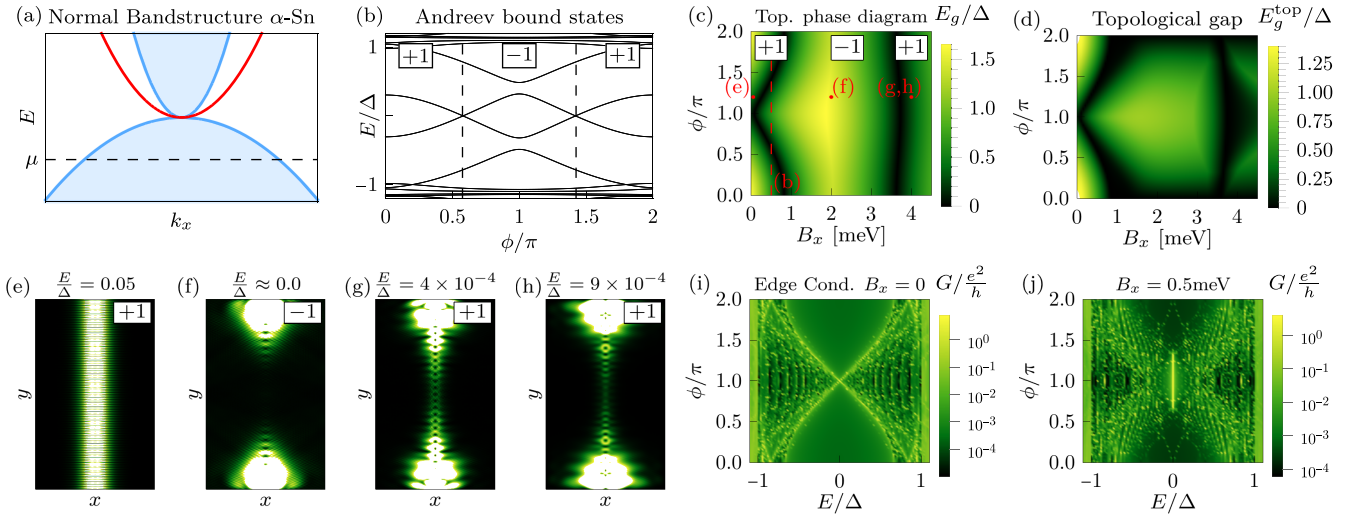


FIG. 3. (a) Band structure of the nonsuperconducting semi-infinite 2D semimetal regime with the bulk continuum (blue shaded) and the edge states (red). The dashed line indicates the chemical potential μ . (b) Andreev bound states as a function of the superconducting phase mismatch ϕ for the Zeeman field $B_x = 0.5$ meV and $k_y = 0$. The dashed lines indicate the topological phase transitions characterized by the topological invariant $\mathcal{Q} = \pm 1$ (framed insets). (c) Energy gap E_g of the Andreev spectrum of the 2D Josephson junction at $k_y = 0$ as a function of ϕ and B_x . The topological regions in the phase diagram are separated by the gap closings (black lines). (d) Topological gap of the Andreev spectrum for all momenta [$E_g^{\text{top}} = \min_{k_y} E_g(k_y)$]. (e)–(h) Density of the lowest energy wave functions in real space for $\phi = 1.2\pi$. (e) Nonlocalized Andreev bound state in the trivial region ($B_x = 0.05$ meV), (f) localized zero-energy Majorana bound state in the topological region ($B_x = 2.0$ meV), and (g) and (h) two localized zero-energy states in the trivial region ($B_x = 4.0$ meV). (i) Conductance calculated at the edge of the N region of the Josephson junction as a function of energy E and ϕ at $B_x = 0$ meV and (j) $B_x = 0.5$ meV with a zero-bias peak in the topological region. Here, we used the parameters for Josephson junction based on α -Sn ($\alpha_0, \alpha_z, \alpha_{\square}$) = (18.62, 11.88, 0) $\frac{\hbar^2}{2m}$ [49], $\mu = -1.0$ meV, while the s -wave induced SC gap is taken for β -Sn with $\Delta = 0.56$ meV [50]. The dimensions of the junction are $W = 20$ nm, $W_S = 150$ nm, and $L = 1000$ nm.

we added a small probe on top of the boundary of the N region, attached to a lead [52], similar as in Ref. [12]. Without magnetic field [Fig. 3(i)], one can clearly see the signal of the degenerate ABSs which cross at $\phi = \pi$. At finite magnetic field [Fig. 3(j)], the ABSs split and host a topological region in between two crossings. The calculated conductance shows a clear zero-bias peak in the topological region, induced by MBSs, which we predict to be observable in future experiments.

We emphasize that the opening of a topological gap is independent of inversion symmetry breaking SOC terms, like BIA and Rashba, in a 2D Josephson junction on Luttinger semimetals. However, our findings are still applicable if such terms are present, as in tetrahedral materials, such as HgTe. Therefore, we predict that any quadratic nodal Luttinger semimetal hosts a MBS in a 2D Josephson junction.

V. CONCLUSIONS AND OUTLOOK

In this paper, we analyze two different Luttinger semimetal systems that host topologically nontrivial properties leading to MBSs. In SC wires, we find two topological transitions for two critical magnetic fields related to light- and heavy-hole band inversions. Interestingly, the range of magnetic fields where topological phase exists is material independent and only determined by the chemical potential. Moreover, we demonstrate that the intrinsic BIA term of any material of the tetrahedral symmetry group is sufficient for a gap opening in

a SC wire, if the magnetic field is applied perpendicular to the wire.

In 2D Josephson junctions, we show that the intrinsic SOC of Luttinger materials in combination with the phase difference of the SCs is sufficient to generate MBSs, even without the application of BIA or Rashba SOC. This opens an avenue for the search of materials which should have intrinsically emergent MBSs. As an example, we propose the experimentally relevant Josephson junction on 2D β -Sn- α -Sn- β -Sn.

Our results could also shed light on the formation of MBSs in other quadratic nodal semimetals, such as $\text{Pr}_2\text{Ir}_2\text{O}_7$ and YPtBi [28,34]. Moreover, the competition between non-SC edge states [see Fig. 3(a)] in the Luttinger semimetal and the formation of MBSs could give rise to physics that can be controlled by the chemical potential. Additionally, we expect interesting features in Josephson junctions on the metallic phase of $j = \frac{3}{2}$ Luttinger systems.

ACKNOWLEDGMENTS

We acknowledge funding by the Deutsche Forschungsgemeinschaft (DFG; German Research Foundation) through SFB 1170, Project-ID 258499086, through the Würzburg-Dresden Cluster of Excellence on Complexity and Topology in Quantum Matter ct.qmat (EXC2147, Project-ID 390858490) as well as by the ENB Graduate School on Topological Insulators. We thank Ralph Claessen, Ion Cosma Fulga, Steffen Schreyeck, and Jonas Erhardt for the enlightening discussions.

- [1] J. Alicea, *Rep. Prog. Phys.* **75**, 076501 (2012).
- [2] C. Beenakker, *Annu. Rev. Condens. Matter Phys.* **4**, 113 (2013).
- [3] R. M. Lutchyn, E. P. A. M. Bakkers, L. P. Kouwenhoven, P. Krogstrup, C. M. Marcus, and Y. Oreg, *Nat. Rev. Mater.* **3**, 52 (2018).
- [4] R. Aguado and L. P. Kouwenhoven, *Phys. Today* **73**(6), 44 (2020).
- [5] E. Prada, P. San-Jose, M. W. A. de Moor, A. Geresdi, E. J. H. Lee, J. Klinovaja, D. Loss, J. Nygård, R. Aguado, and L. P. Kouwenhoven, *Nat. Rev. Phys.* **2**, 575 (2020).
- [6] A. Kitaev, *Ann. Phys.* **303**, 2 (2003).
- [7] M. Leijnse and K. Flensberg, *Semicond. Sci. Technol.* **27**, 124003 (2012).
- [8] L. Fu and C. L. Kane, *Phys. Rev. Lett.* **100**, 096407 (2008).
- [9] G. Goldstein and C. Chamon, *Phys. Rev. B* **84**, 205109 (2011).
- [10] V. Mourik, K. Zuo, S. M. Frolov, S. R. Plissard, E. P. A. M. Bakkers, and L. P. Kouwenhoven, *Science* **336**, 1003 (2012).
- [11] M.-T. Deng, S. Vaitiekenas, E. Prada, P. San-Jose, J. Nygård, P. Krogstrup, R. Aguado, and C. M. Marcus, *Phys. Rev. B* **98**, 085125 (2018).
- [12] H. Ren, F. Pientka, S. Hart, A. T. Pierce, M. Kosowsky, L. Lunczer, R. Schlereth, B. Scharf, E. M. Hankiewicz, L. W. Molenkamp *et al.*, *Nature (London)* **569**, 93 (2019).
- [13] A. Fornieri, A. M. Whiticar, F. Setiawan, E. Portolés, A. C. C. Drachmann, A. Keselman, S. Gronin, C. Thomas, T. Wang, R. Kallaher *et al.*, *Nature (London)* **569**, 89 (2019).
- [14] R. M. Lutchyn, J. D. Sau, and S. Das Sarma, *Phys. Rev. Lett.* **105**, 077001 (2010).
- [15] Y. Oreg, G. Refael, and F. von Oppen, *Phys. Rev. Lett.* **105**, 177002 (2010).
- [16] R. Wakatsuki, M. Ezawa, and N. Nagaosa, *Phys. Rev. B* **89**, 174514 (2014).
- [17] P. Szumniak, D. Chevallier, D. Loss, and J. Klinovaja, *Phys. Rev. B* **96**, 041401(R) (2017).
- [18] M. Kharitonov, E. M. Hankiewicz, B. Trauzettel, and F. S. Bergeret, *Phys. Rev. B* **104**, 134516 (2021).
- [19] Y. Peng, F. Pientka, E. Berg, Y. Oreg, and F. von Oppen, *Phys. Rev. B* **94**, 085409 (2016).
- [20] F. Pientka, A. Keselman, E. Berg, A. Yacoby, A. Stern, and B. I. Halperin, *Phys. Rev. X* **7**, 021032 (2017).
- [21] B. Scharf, F. Pientka, H. Ren, A. Yacoby, and E. M. Hankiewicz, *Phys. Rev. B* **99**, 214503 (2019).
- [22] J. Ruan, S.-K. Jian, H. Yao, H. Zhang, S.-C. Zhang, and D. Xing, *Nat. Commun.* **7**, 11136 (2016).
- [23] M. Kharitonov, J.-B. Mayer, and E. M. Hankiewicz, *Phys. Rev. Lett.* **119**, 266402 (2017).
- [24] C. Brüne, C. X. Liu, E. G. Novik, E. M. Hankiewicz, H. Buhmann, Y. L. Chen, X. L. Qi, Z. X. Shen, S. C. Zhang, and L. W. Molenkamp, *Phys. Rev. Lett.* **106**, 126803 (2011).
- [25] Y. Baum, J. Böttcher, C. Brüne, C. Thienel, L. W. Molenkamp, A. Stern, and E. M. Hankiewicz, *Phys. Rev. B* **89**, 245136 (2014).
- [26] C. Brüne, C. Thienel, M. Stuber, J. Böttcher, H. Buhmann, E. G. Novik, C.-X. Liu, E. M. Hankiewicz, and L. W. Molenkamp, *Phys. Rev. X* **4**, 041045 (2014).
- [27] T. Morimoto and A. Furusaki, *Phys. Rev. B* **89**, 235127 (2014).
- [28] T. Kondo, M. Nakayama, R. Chen, J. J. Ishikawa, E.-G. Moon, T. Yamamoto, Y. Ota, W. Malaeb, H. Kanai, Y. Nakashima *et al.*, *Nat. Commun.* **6**, 10042 (2015).
- [29] D. Zhang, H. Wang, J. Ruan, G. Yao, and H. Zhang, *Phys. Rev. B* **97**, 195139 (2018).
- [30] Sayed Ali Akbar Ghorashi, P. Hosur, and C.-S. Ting, *Phys. Rev. B* **97**, 205402 (2018).
- [31] I. Boettcher and I. F. Herbut, *Phys. Rev. B* **93**, 205138 (2016).
- [32] I. Boettcher and I. F. Herbut, *Phys. Rev. Lett.* **120**, 057002 (2018).
- [33] P. M. R. Brydon, L. Wang, M. Weinert, and D. F. Agterberg, *Phys. Rev. Lett.* **116**, 177001 (2016).
- [34] H. Kim, K. Wang, Y. Nakajima, R. Hu, S. Ziemak, P. Syers, L. Wang, H. Hodovanets, J. D. Denlinger, P. M. R. Brydon *et al.*, *Sci. Adv.* **4**, eaao4513 (2018).
- [35] B. Roy, Sayed Ali Akbar Ghorashi, M. S. Foster, and A. H. Nevidomskyy, *Phys. Rev. B* **99**, 054505 (2019).
- [36] H. Kim, J. Lee, H. Hodovanets, K. Wang, J. D. Sau, and J. Paglione, *arXiv:2010.12085*.
- [37] P. Dutta, F. Parhizgar, and A. M. Black-Schaffer, *Phys. Rev. Research* **3**, 033255 (2021).
- [38] C. Timm and A. Bhattacharya, *Phys. Rev. B* **104**, 094529 (2021).
- [39] M. Bahari, S.-B. Zhang, and B. Trauzettel, *Phys. Rev. Research* **4**, L012017 (2022).
- [40] R. Winkler, *Spin–Orbit Coupling Effects in Two-Dimensional Electron and Hole Systems*, Springer Tracts in Modern Physics Vol. 191 (Springer, Berlin, Heidelberg, 2003).
- [41] W. Kohn and J. M. Luttinger, *Phys. Rev.* **96**, 529 (1954).
- [42] A. P. Schnyder, S. Ryu, A. Furusaki, and A. W. W. Ludwig, *Phys. Rev. B* **78**, 195125 (2008).
- [43] S. Ryu, A. P. Schnyder, A. Furusaki, and A. W. Ludwig, *New J. Phys.* **12**, 065010 (2010).
- [44] A. R. Akhmerov, J. P. Dahlhaus, F. Hassler, M. Wimmer, and C. W. J. Beenakker, *Phys. Rev. Lett.* **106**, 057001 (2011).
- [45] I. C. Fulga, F. Hassler, A. R. Akhmerov, and C. W. J. Beenakker, *Phys. Rev. B* **83**, 155429 (2011).
- [46] C. W. Groth, M. Wimmer, A. R. Akhmerov, and X. Waintal, *New J. Phys.* **16**, 063065 (2014).
- [47] E. G. Novik, A. Pfeuffer-Jeschke, T. Jungwirth, V. Latussek, C. R. Becker, G. Landwehr, H. Buhmann, and L. W. Molenkamp, *Phys. Rev. B* **72**, 035321 (2005).
- [48] M. Cardona, N. E. Christensen, and G. Fasol, *Phys. Rev. Lett.* **56**, 2831 (1986).
- [49] O. Madelung, *Semiconductors: Data Handbook* (Springer-Verlag, Berlin Heidelberg, 2004).
- [50] N. W. Ashcroft and N. D. Mermin, *Solid State Physics* (Holt-Saunders, Philadelphia, 1976).
- [51] J. Hajer, M. Kessel, C. Brüne, M. P. Stehno, H. Buhmann, and L. W. Molenkamp, *Nano Lett.* **19**, 4078 (2019).
- [52] See Supplemental Material at <http://link.aps.org/supplemental/10.1103/PhysRevB.105.224513> for the Luttinger Hamiltonian in a rotated basis to emphasize the intrinsic spin-orbit coupling in two dimensions and describe the method to calculate the edge conductance of Figs. 3(i) and 3(j).
- [53] T. Fukui, K. Shiozaki, T. Fujiwara, and S. Fujimoto, *J. Phys. Soc. Jpn.* **81**, 114602 (2012).
- [54] We estimate the coherence length in the SC regions to be $\xi = \frac{\hbar v_F}{\Delta} = 50.0$ nm.
- [55] M. Hell, M. Leijnse, and K. Flensberg, *Phys. Rev. Lett.* **118**, 107701 (2017).